

PREDICTIONS FOR THE COUNTS OF FAINT, HIGH-REDSHIFT GALAXIES IN THE MID-INFRARED

ZOLTÁN HAIMAN¹, DAVID N. SPERGEL, AND EDWIN L. TURNER
Princeton University Observatory, Princeton, NJ 08544, USA
zoltan,dns,elt@astro.princeton.edu

Draft version October 24, 2018

ABSTRACT

Deep mid-infrared (MIR) observations could reveal a population of faint, high-redshift ($z > 3$) dusty starburst galaxies that are the progenitors of present-day spheroids or bulges, and are beyond the reach of current instruments. We utilize a semi-analytic galaxy formation scheme to find an extreme model for the MIR galaxy counts, designed to maximize the number of detectable sources down to a flux level of a few nJy. The model incorporates the formation of heavily dust-enshrouded stellar populations at high redshift, and is consistent with existing observations, including faint counts at $1.6\mu\text{m}$ in the NICMOS Hubble Deep Field, and the upper limit on the extragalactic MIR background from TeV gamma rays. Our models predict upto ~ 0.5 galaxies/arcsec² at the threshold of 100 nJy at $6\mu\text{m}$, with a comparable or larger surface density at longer MIR wavelengths. We conclude that a significant new population of high-redshift galaxies could be detected by the *Space Infrared Telescope Facility (SIRTF)* and *Next Generation Space Telescope (NGST)*. Such a population would constitute background noise for the *Terrestrial Planet Finder (TPF)*, and could necessitate repeat observations: every *TPF* resolution element have a $\sim 10\%$ chance of being contaminated by a background galaxy.

Subject headings: cosmology: theory – early universe – galaxies: formation – galaxies: ISM

1. INTRODUCTION

The past few years have seen significant progress in probing the ultra-high redshift universe, with both galaxies (Dey et al. 1998; Weymann et al. 1998; Spinrad et al. 1998; Hu et al. 1999) and quasars (Fan et al. 1999, 2000, 2001; Zheng et al. 2000; Stern et al. 2000) being discovered in increasing numbers well beyond redshift $z = 5$. In hierarchical structure formation scenarios in cold dark matter (CDM) cosmologies, the first baryonic objects appear at still higher redshifts: at $z \approx 20 - 30$, when the first high- σ peaks collapse near the Jeans scale of $\sim 10^5 M_\odot$ (Haiman, Thoul & Loeb 1996; see Barkana & Loeb 2001 for a recent review). Radiative cooling is efficient in the dense gas that has collapsed on these scales, and in principle, it can facilitate efficient star-formation. Indeed, significant activity must have taken places at high redshifts, in order to reionize the intergalactic medium (IGM) by $z \gtrsim 6$, and enrich it with metals by $z \gtrsim 4$.

The deepest detections of galaxies and quasars to date have been obtained at optical or near infrared (NIR) wavelengths, where the objects were identified in broad-band filters by their continuum, or in narrow-band imaging observations by their Lyman- α emission. The *Next Generation Space Telescope (NGST)* will be able to extend these observations to $\gtrsim 32$ mag in the $1 - 5\mu\text{m}$ wavelength range, and detect mini-galaxies and mini-quasars at redshifts $z \gtrsim 10$. The expected number of faint sources in future, deep NIR observations have been studied extensively in the context of hierarchical structure formation, using simple semi-analytic models. Haiman & Loeb (1997; 1998) showed that if halos collapsing at high redshifts have reasonable star (or quasar black hole, BH) formation efficiencies, they can then be detected in the NIR

continuum in great numbers, with surface densities possibly reaching ~ 1000 sources per arcmin⁻². Similarly large numbers of high-redshift objects could be detected through optical/NIR narrow band filters or spectroscopic imaging. The counts have been computed and found to be potentially significant for Ly α emission originating either from a usual stellar population (Haiman & Spaans 1999) or from the release of gravitational binding energy (Haiman, Spaans & Quataert 2000). In addition, recombination lines of helium fall into the optical/NIR, allowing the detection of high-redshift sources, provided they have sufficiently hard spectra (Tumlinson & Shull 2001; Oh & Haiman 2001).

Observations at nearby redshifts have revealed that spheroid systems – the bulges of disk galaxies, as well as dwarf spheroidal galaxies – have exceedingly old stellar populations (see, e.g. Binney & Tremaine 1987). It is natural to assume that these objects formed at high redshifts. At the epoch when the halos harboring these objects first assembled, gas supply was likely plentiful, resulting in high star formation rates. In analogy with local starburst galaxies, these high-redshift bursts of star formation were likely heavily dust enshrouded, with unusually red spectra enhancing fluxes at longer wavelengths. In this paper, our goal is to quantify this scenario, and to predict the counts of faint, high-redshift galaxies at mid-IR (MIR) wavelengths.

Semi-analytic galaxy formation models, originally applied at optical wavelengths (Kauffmann & White 1993) have recently been extended to the far-infrared (FIR), and all the way to sub-mm range. The key to such extensions is the availability of template spectra that incorporate the absorption and re-emission of starlight by dust.

¹Hubble Fellow

Dusty galaxy models have successfully matched spectra of known starburst galaxies (Gordon et al. 1997), as well as a broader range of galaxy types (Silva et al. 1998; Devriendt et al. 1999). When combined with hierarchical galaxy-formation schemes, such spectral models have also successfully reproduced the existing IR/sub-mm luminosity functions (Guiderdoni et al. 1998; Silva et al. 1999), and have been used to investigate several aspects of IR galaxies, such as the faint-end slope of their luminosity function, and the abundance of ultra-luminous infrared galaxies (ULIRGs, Devriendt & Guiderdoni 2000).

In the present paper, we consider the number counts of faint, high redshift sources at MIR wavelengths, using similar semi-analytic models. The main difference between the present paper and previous studies is that we extrapolate the models down to a very faint flux level. Our study is motivated primarily by the forthcoming instruments *NGST*, the *Space Infrared Telescope Facility (SIRTF)*, and the *Terrestrial Planet Finder (TPF)*. It is likely that *NGST* will have very deep (~ 100 nJy) imaging capability in the MIR out to $\lambda \sim 30\mu\text{m}$ (Serabyn et al. 1999). In very long exposure 10^6 s observations, *SIRTF* could reach similar limiting fluxes; while ~ 100 nJy is also the target flux level for the IR version of *TPF* to discover Earth-like planets at a distance of 10pc.

Observations in the MIR have only been possible in a few narrow bands from the ground, and the deepest existing surveys from space, i.e. by the *Infrared Space Observatory (ISO)*, are still relatively shallow, achieving completeness only down to ~ 0.1 mJy (see, e.g. Franceschini 2000 for a review). We use the models to obtain counts to the much fainter flux levels of ~ 1 nJy. We emphasize that this is a very significant extrapolation from current data, by several orders of magnitude. Such extrapolations are inevitably uncertain. In particular, we do not attempt here to present a “most likely” model. Instead, the goal of the present paper is to produce “extreme” models that *maximize* the MIR counts at ~ 100 nJy, but are (1) consistent with all existing observations, and (2) are not obviously physically unrealistic. These predictions will serve as a guide to the most optimistic scenario for detecting ultra-faint galaxies with *NGST*, *SIRTF*, and *TPF*. In addition, these calculations will be useful to assess whether these observations may reach the MIR confusion limit.

The rest of this paper is organized as follows. In §2, we describe the ingredients of our modeling, including the presence of dust, and discuss the relevant observational constraints. In §3, we present the counts at different MIR wavelengths, describe the properties of the faint sources, such as typical masses and redshift distributions, and discuss the confusion limit. Finally, in §4, we summarize our conclusions and the implications of this work. Throughout this paper, we assume a flat Λ CDM cosmology with the parameters $(\Omega_m, \Omega_\Lambda, \Omega_b h^2, h, \sigma_{8h^{-1}}) = (0.3, 0.7, 0.019, 0.7, 1.0)$.

2. MODEL DESCRIPTION

Our semi-analytical approach is a simplified version of the Monte-Carlo models found in the literature of hierarchical galaxy formation (Kauffmann & White 1993, Lacey & Cole 1993; for a more recent application to high-redshift galaxies, see Haiman & Loeb 1997, 1998; Wechsler et al.

2001). Its three main aspects are (1) the distribution of dark matter halos; (2) the template spectra and light-curves of the stellar populations; and (3) the calibration of the star-formation efficiency. In this section, we describe our treatment of each of these issues in turn.

2.1. Dark Matter Halos

We assume that galaxies form in dark matter halos, whose abundance $dN/dM(M, z)$ follows the standard Press & Schechter (1974; hereafter PS) mass function. The cosmological power spectrum is computed from the fitting formulae of Eisenstein & Hu (1999), and we set $\delta_c = 1.68$ for the usual critical overdensity for collapse. In the extended PS formalism, it is also possible to compute the distribution of ages for halos of a given mass and redshift. Here we define the age of a halo to be the time elapsed since the halo first acquired half of its mass, and follow equation 2.26 in Lacey & Cole (1993; hereafter LC) to obtain the halo age-distribution $dp/dt(M, z)$. We assume further that the age of the stellar population in the halo equals the age of the halo.

It is important to emphasize that improvements have been made over the PS mass function, taking into account the lack of spherical symmetry, and that large-scale three-dimensional simulations have possibly uncovered significant differences in the abundance of high- σ objects (e.g., Sheth, Mo & Tormen 2001; Jenkins et al. 2001). Our main motivation for the choosing the standard PS mass function is “technical”: the semi-analytical derivation of dp/dt is only applicable for the mass function in the standard PS theory; at present no analogous derivation exists for the improved mass functions. However, we note that the typical objects we will be interested in below have halo masses corresponding to $\lesssim 3.5\sigma$ density peaks. At these masses, the discrepancy between the PS mass function and the simulations is within a factor of \sim three, with the PS formula under-predicting the abundance. Hence, we expect that if we were able to use the improved mass function (e.g. equation 9 in Jenkins et al. 2001), at any given flux and at the highest redshifts, the number of sources we predict could increase by upto a factor of \sim three (or alternatively, we would predict the same number of sources for a \sim three times lower star-formation efficiency).

2.2. Template Spectra and the Effects of Dust

Another ingredient of our model is the template spectrum emitted by high-redshift galaxies. Standard population synthesis models have been successful in matching the optical/NIR spectra of observed nearby galaxies (see Leitherer et al. 1999 for a review), and have often been adopted in semi-analytical galaxy formation models. Closest to the present context is the study of counts at high redshifts focusing on these wavelengths (e.g. Haiman & Loeb 1997; 1998). However, as mentioned above, the effects of dust can become conspicuous in the MIR regime at wavelengths $\lambda \sim$ few μm , and the importance of dust increases for still longer wavelengths. Furthermore, studies of the spatial distribution and optical properties of dust in nearby starburst galaxies have shown that models with a simple “foreground screen” of “normal” dust (with a cross-section similar to that of dust in the Milky Way or

the Magellanic Clouds) is inconsistent with the data (for a recent example, see Gordon et al. 1997). The inferences have been that the stars and the dust must have different spatial distributions and temporal evolutions.

The presence of dust therefore adds considerable complexity to spectral modeling. Several recent studies have addressed the problem of dusty galaxy spectra (e.g. Silva et al. 1998; Devriendt et al. 1999; Charlot & Fall 2000). The main typical features of successful models are that the dust is concentrated in dense star-forming clouds, and therefore it has a highly patchy distribution compared to the overall stellar distribution. In addition, star-forming clouds have a finite lifetime, making the effects of dust time-dependent. The properties of the grains themselves have also been found to be important in the MIR. In particular, models for the size-distribution and cross-section of grains accurately describe the optical/UV properties of Galactic dust (Draine & Lee 1984), but an additional hot dust component, requiring the presence of very small grains or PAH molecules, is needed to reproduce the observed spectra in the range $2\mu\text{m} \lesssim \lambda \lesssim 30\mu\text{m}$ (e.g., Puget et al. 1985).

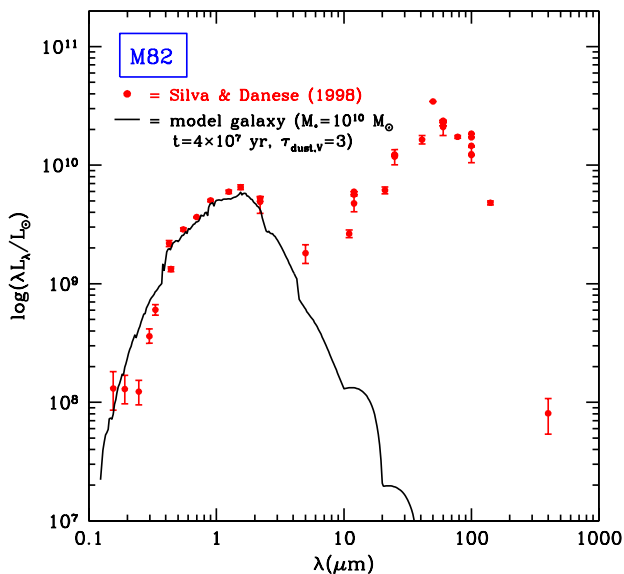


Fig. 1.— The spectrum of M82, a dusty starburst galaxy in the local universe, is reproduced by a $9 \times 10^9 M_{\odot}$ (stellar mass), and 4×10^7 yr old model galaxy upto $\sim 5\mu\text{m}$. The model does not include dust emission, and under-predicts the flux at longer wavelengths.

As emphasized by Charlot & Fall (2000), as a result of these complications, a simple foreground dust screen can not be assumed. However, these authors derive a simple phenomenological recipe for the effects of dust, which they find has an “effective” foreground-screen absorption curve proportional to $\lambda^{-0.7}$ (i.e. grey compared to Draine & Lee). In most of our calculations below, we adopt this simple power-law absorption cross section. The overall normalization is still largely ad-hoc, and is likely to vary from galaxy to galaxy. However, here we chose the value such that $\tau_{\text{dust}} = 3(\lambda/5500\text{\AA})^{-0.7}$, i.e. we set the opacity in the visual band to be ~ 3 . By assumption, this will

then represent the typical dust content of high-redshift starburst galaxies. This value is similar to that inferred for the local starburst galaxy M82 (e.g. Silva et al. 1998; Devriendt et al. 1999). In Figure 1, we combine the dust-free stellar synthesis models of Bruzual & Charlot (2000) and a foreground screen of dust with this opacity. The resulting spectrum provides an excellent fit to the spectrum of M82 upto a wavelength of $\sim 5\mu\text{m}$. In this figure, we have assumed a single burst of star formation with a stellar mass of $9 \times 10^9 M_{\odot}$, and an age of 4×10^7 yr for the stellar population.

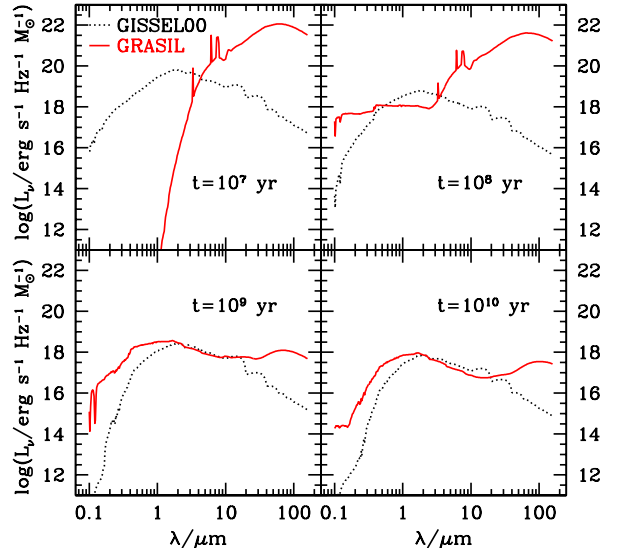


Fig. 2.— Comparison of time-evolving template spectra adopted for galaxies, under two different assumptions. The solid curves, labeled GISSSEL00, represent a model in which a dust-free population synthesis model is combined with a foreground screen of dust with an effective absorption law $\propto \lambda^{-0.7}$, as suggested by Charlot & Fall (2000). The dashed curves, labeled GRASIL, is based on the detailed model spectra of a dusty starburst galaxy, using the computer code of Silva et al. (1998). The two models differ significantly at early stages ($t \lesssim 10^8$ yr), but predict similar MIR spectra at late times.

An obvious shortcoming of this simple model is that it does not include dust emission, and therefore under-predicts the flux at wavelengths $\lambda \gtrsim 5\mu\text{m}$. However, we have verified explicitly that the total amount of energy absorbed by the dust in the UV approximately equals the observed FIR emission. Therefore at least energetically, our simplistic model is viable, although it may prove difficult to produce the observed SN rate and line emission (see Silva et al. 1998). In order to make a more realistic model, and in which we are also able to compute galaxy counts at longer wavelengths, we utilized the publicly available program GRASIL². The program computes the emergent time-dependent spectrum from a galaxy, under the assumptions of patchy dust distribution (see Silva et al. 1998 for the description of their model). Here we used it to follow the evolution of the spectrum after a

²Downloadable directly from <http://grana.pd.astro.it>

single burst of dusty star formation, with the following parameters (cf. Tables 1 and 2 in Silva et al. 1998): $M_G = 1.8 \times 10^{10} M_\odot$ (total gas mass), $t_{\text{inf}} = 10^7$ yr (gas infall timescale), $f_{\text{mc}} = 0.08$ (mass fraction of gas in star-forming clouds that contribute most of the dust opacity), $r_{\text{mc}} = 16$ pc, $M_{\text{mc}} = 10^6 M_\odot$, $t_0 = 5.7 \times 10^7$ yr (radius, mass, and dispersion timescale of star-forming clouds), $r_c^* = 0.15$ kpc, $r_c^c = 0.15$ kpc (core radii of star and gas distribution, both for a King profile). We then assumed that the normalization of the emitted flux scales linearly with the total gas mass M_G (this implicitly requires that all length-scales scale as $M_G^{1/3}$). This assumption allows us to assign a time-dependent emission spectrum to a dark halo once its age and star formation efficiency is specified. A more accurate interfacing of the template spectra with the hierarchical galaxy formation models could include a non-linear scaling between spectrum and galaxy mass (Silva et al. 1999).

For reference, we show the time-evolving template spectrum of a model galaxy, per unit solar mass in stars, in Figure 2. The spectra are shown both under the assumption of an effective foreground screen in a Bruzual-Charlot model (labeled GISSEL00), and using the code GRASIL. It is apparent that the two models predict quite different MIR spectra at early times ($t \lesssim 10^8$ yr). This stems from the fact that in the GRASIL model, the initial starburst is heavily dust-enshrouded. Nearly all of the starlight $\lambda \lesssim 5 \mu\text{m}$ is absorbed by dust in molecular clouds, and re-emitted at long wavelengths, until the star-forming clouds disperse and the dust opacity is significantly reduced (at $t \gtrsim t_0$). At late times, the two models agree fairly well in the MIR range ($5 \mu\text{m} \lesssim \lambda \lesssim 30 \mu\text{m}$), although at the longest wavelengths, the GRASIL models still predict a larger flux.

2.3. Calibration of Star-formation Efficiency, and Existing Constraints

The final ingredient of our model is the calibration of the star-formation efficiency in the dark halos. Although this could vary significantly from galaxy to galaxy, for simplicity we assume here that all halos of a given velocity dispersion turn the same amount of gas into stars. There are several approaches to choosing a calibration. When fitting existing data, such as galaxy counts, then the efficiencies can be chosen to be the best-fitting values (e.g. Kauffmann & White 1993). In the models of Haiman & Loeb (1997, 1998) that extrapolate to high redshifts, the star-formation efficiency was normalized based on the mean metallicity of the high-redshift Ly α forest.

In the present work, our aim is to maximize high-redshift galaxy counts. Accordingly, we regard the overall normalization of the starformation efficiency as a free parameter, and we set it to its maximum allowed value based on existing constraints (see discussion below). We envision that the remnants of the high-redshift starbursts can be identified with the spheroid components in local galaxies. Accordingly, based on the Faber-Jackson relation, we adopt the scaling $M_{\text{star}} \propto \sigma_{\text{halo}}^4$, where M_{star} is the mass in turned into stars, and σ_{halo} is the velocity dispersion of the host halo. We then normalize the models as follows:

$$\left(\frac{\sigma_{\text{halo}}}{115 \text{ km s}^{-1}} \right)^4 = \left(\frac{M_{\text{star}}}{4.5 \times 10^{11} M_\odot} \right) \quad (1)$$

In addition, we postulate that no stars form in halos with velocity dispersions less than 30 km s^{-1} , because of the presence of the UV background (see, e.g., Navarro & Steinmetz 1997). Prior to reionization (which we here assume to occur at redshift $z = 10$), we lower this threshold to 11.7 km s^{-1} , corresponding to a virial temperature of 10^4 K , where this cutoff is determined by the requirement of efficient cooling, rather than the feedback from the UV background (e.g. Haiman, Abel & Rees 2000). We also note that equation (1) corresponds to a ~ 3 times higher normalization of the Faber-Jackson relation than derived for the bulges of local spiral galaxies (Whitmore, Kirshner & Schechter 1979).

Using the standard relation between halo velocity dispersion and mass (e.g. Navarro, Frenk & White 1997), and assuming that the gas available for star formation is $M_{\text{gas}} = (\Omega_b/\Omega_m)M_{\text{halo}}$ the stellar mass here corresponds nominally to $M_{\text{star}} \sim 6 - 7 \times M_{\text{gas}}$ (for the typical halos at each observed flux). Hence our maximal model is rather extreme, in that it assumes the formation of $\gtrsim 6-7$ generations of massive stars, formed in quick succession, to recycle the available gas into stars 6-7 times (for reference, we note that the models in HL97 had the much lower overall star formation efficiencies of $M_{\text{star}}/M_{\text{gas}} \sim 2-20\%$). A stellar population with a Salpeter IMF would return only $\approx 30\%$ of its mass to the interstellar medium in $\sim 3 \times 10^8$ yr, and would allow recycling of the gas only \sim twice. The requirement in our model of 6-7 cycles could be achieved either with a flatter IMF (since massive stars return essentially all their mass; and IMF slope of ~ 1.8 instead of 2.35 is then required), or by postulating a larger gas reservoir for a system with a given velocity dispersion. Note that significant metal enrichment, to solar levels, implies that ~ 8 generations of star-formation did indeed take place in the Milky Way (e.g. Binney & Tremaine 1987), and observed heavy element abundances in galaxy clusters also favor significant enrichment at high redshifts (Renzini 1997).

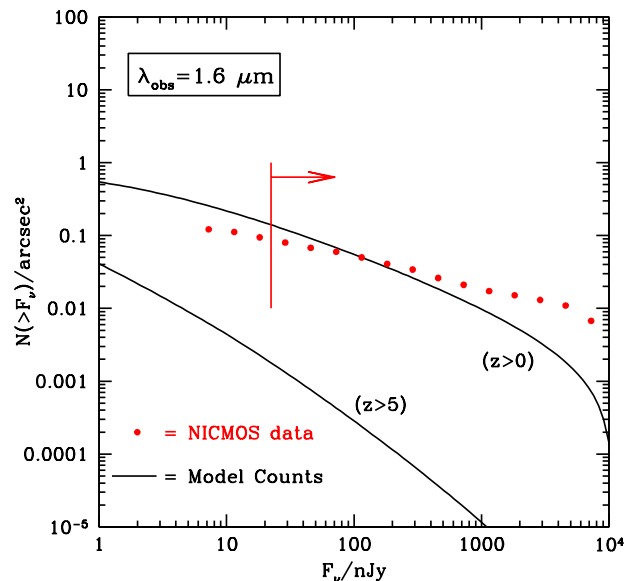


Fig. 3.— Cumulative number counts of galaxies at $1.6 \mu\text{m}$ brighter than a given flux threshold F_ν . The upper solid curve shows all galaxies, and the lower curve shows only

those beyond redshift $z = 5$. The data-points are from NICMOS observations covering $1/8^{\text{th}}$ of the area of the Hubble Deep Field North (Thompson et al. 1999). Our models are consistent with these counts, owing to the large dust opacity (and therefore red spectra) that we adopted.

Existing MIR counts (from *ISOCAM*) extend down only to about $\sim 0.1\text{mJy}$ (Franceschini 2000; Franceschini et al. 1997; Clements et al. 1999), and we extrapolate the models to several orders of magnitude fainter flux levels. Nevertheless, our normalization has to be consistent with faint galaxy counts in the Hubble Deep Field (HDF) in both optical and NIR bands. In particular, we found that the most constraining HDF data are the $1.6\mu\text{m}$ galaxy counts in a NICMOS follow-up observation of $\sim 1/8^{\text{th}}$ of the HDF area (Thompson et al. 1999). This deep survey has a 50% completion limit near 28^{th} mag, and has detected a total of ~ 300 sources. We have found that models with the template spectra described in § 2.2 that are consistent with this abundance always satisfy the limits from optical/UV counts in the Hubble Deep Field to about the same depth. In Figure 3 we show the $1.6\mu\text{m}$ counts in our models using the GISEL spectral models, and with the normalization in equation (1). The upper curve shows all sources, the lower curve shows only the sources beyond redshift $z = 5$, and the dots show the NICMOS data. The figure explicitly demonstrates that our model is marginally consistent with the NICMOS counts.

An integral constraint on the MIR counts can also be obtained from the upper limit on the total cosmic infrared background energy density. The latter limit derives from the TeV gamma ray spectrum of the blazar Mrk 501, observed in its high state with HEGRA, yielding a stringent limit on the optical depth to pair production at TeV energies (Stanev & Franceschini 1998; Dwek 2001). The upper limit on the MIR background at $6\mu\text{m}$ is $\sim 10^4\text{Jy sr}^{-1}$. In Figure 4 below, we show as the dashed curve the ratio of the flux from all sources brighter than some flux F_ν to this upper limit. The figure shows that our maximal model, which is marginally consistent with the $1.6\mu\text{m}$ NICMOS counts, is also marginally consistent with the upper limit on the MIR background.

3. RESULTS AND DISCUSSION

In this section, we present the galaxy counts at different MIR wavelengths, describe the properties of the faint sources such as typical masses and redshift distributions, and discuss the confusion limit for *TPF*.

3.1. Mid-IR Galaxy Counts

Figure 4 shows the cumulative galaxy counts at $6\mu\text{m}$ in our model, using the effective dust opacity prescription from Charlot & Fall (2000), superimposed on the dust-free spectral model from GISEL00 (Bruzual & Charlot 2000). The upper solid curve shows all galaxies, and the lower curve shows only those beyond redshift $z = 5$. The dashed curve shows the contribution of the sources to the upper limit on the $6\mu\text{m}$ background, as discussed above.

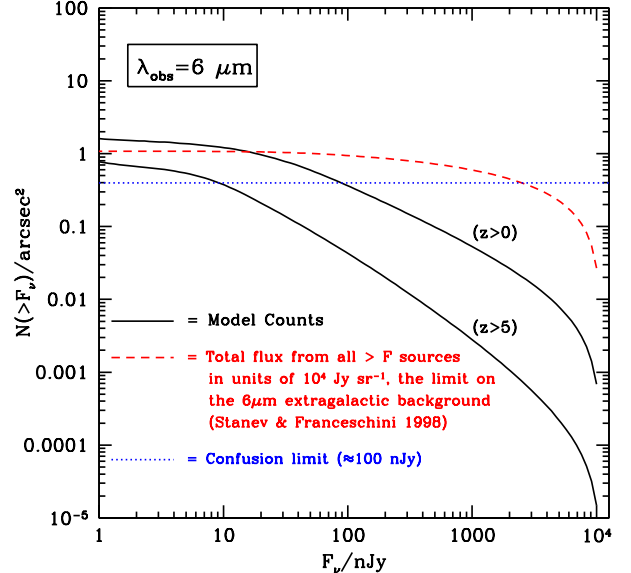


Fig. 4.— Cumulative galaxy counts at $6\mu\text{m}$. The upper solid curve shows all galaxies, and the lower curve shows galaxies beyond redshift $z = 5$. The dashed curve shows the ratio of the total flux from all sources brighter than the flux F_ν to the upper limit on the background, 10^4Jy sr^{-1} (Stanev & Franceschini 1998). The model is consistent with this upper limit. The dotted curve shows the confusion limit expected from a MIR version of the *TPF*.

The most striking feature shown in Figure 4 is the large number of galaxies. At the flux threshold of 100 nJy , over 1000 sources are predicted per arcmin^{-2} . The flattening of the counts between ~ 10 and $\sim 20\text{ nJy}$ is due to the lower limit we imposed (§ 2.3) on the velocity dispersion of halos that are able to host galaxies. It is worth emphasizing again that the deepest data from *ISO* only reaches the comparatively shallow flux threshold of $\sim 0.1\text{mJy}$ (at $6.7\mu\text{m}$ and $15\mu\text{m}$). In fact, the *ISO* counts (at $15\mu\text{m}$) appear to show a significant flattening from 1mJy to $\sim 0.1\text{mJy}$. This, however, is not inconsistent with a significant re-steepening of the counts at fainter fluxes, revealing a new population as predicted by our models.

This new population of faint, dusty, high-redshift galaxies could be uncovered by *SIRTF*, although reaching the flux level of 100 nJy for a $S/N=5$ detection of a point source requires an integration time of several $\times 10^5$ seconds (Simpson & Eisenhardt 1999). *NGST* will be able to reach the same sensitivity in a $\sim 10^4$ seconds out to $\sim 10\mu\text{m}$, and in $\sim 10^6$ seconds out to $\sim 30\mu\text{m}$, while a “*NGST* Deep Field” with a 10^6s exposure could reach fluxes as faint as a few nJy out to $\sim 10\mu\text{m}$. The flux threshold of 100 nJy has also been chosen as the target flux for the MIR version of *TPF*, based on its mission goal to detect Earth-like planets at a distance of 10 pc .³

³See <http://sirtf.caltech.edu>, <http://www.ngst.nasa.gov>, and <http://tpf.jpl.nasa.gov> for quantitative discussions of the sensitivities.

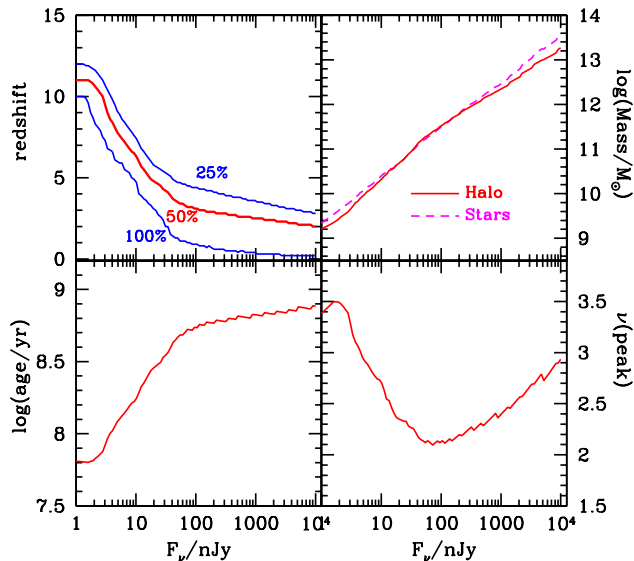


Fig. 5.— Characteristic properties of the dusty sources that make up the counts in Figures 3 and 4: (a) redshifts above which sources make up 25, 50, and 100% of the total observed counts; (b) masses of objects at the 50% redshift cut; (c) typical stellar ages; and (d) rarity of the host density peaks in units of r.m.s. primordial density fluctuation σ_M .

The characteristic properties of the sources making up the counts in Figures 3 and 4 are summarized by the four panels of Figure 5. In the top left panel, we illustrate the redshift distribution of the sources as a function of their $6\mu\text{m}$ flux, by showing the redshifts at each flux beyond which sources make up a fraction 25, 50, and 100% of the observed counts. The low-redshift cutoff is a result of the limit we imposed on the circular velocities of halos harboring active galaxies. The redshift distribution for fainter sources is clearly biased to higher redshifts, with an apparent upturn in the typical redshift below $\sim 100\text{nJy}$. While approximately a half of the 100nJy sources are located at $z > 3$, all of the 1nJy sources are at $z > 10$. In the top right panel, we show the mass of stars that have been converted to stars in the halos at the 50% redshift cut, together with the masses of their host halos. This explicitly demonstrates the high starformation rates in our models, using up a nominal amount of gas nearly equal to the halo mass – implying multiple generations of starformation. The bottom left panel shows the ages of the sources at the 50% redshift cut. These are between $10^8 - 10^9\text{yr}$, with the fainter sources systematically younger. Finally, the bottom right panel shows the rarity of the density peaks hosting the halos at the 50% redshift cut, in units of the r.m.s. primordial density fluctuation σ_M . The typical sources correspond to $2-3\sigma$ peaks in the primordial density field.

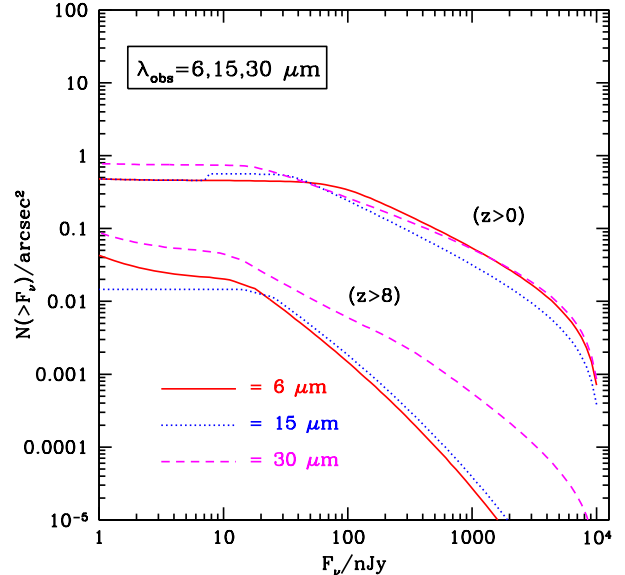


Fig. 6.— Source counts as in Figure 4 but including longer MIR wavelengths. To compute these counts, we have used the program GRASIL (Silva et al. 1998) for the spectra of dusty starbursts, which includes re-emission of starlight by hot dust. The model is normalized to predict the same $6\mu\text{m}$ counts as in the simplified model in Figure 4. At higher redshifts, longer MIR wavelengths are advantageous, and can reveal an increasingly larger number of galaxies.

In Figure 6 we show the cumulative galaxy counts at longer wavelengths, using the dust models computed with the GRASIL code. We have re-normalized the starformation efficiency in the GRASIL-based models so that they predict essentially the same $6\mu\text{m}$ counts as obtained in the simplified effective dust-screen model in Figure 4. We found that this corresponds to a reduction of the starformation efficiency by a factor of ~ 3 relative to equation (1). The counts at $6\mu\text{m}$, $15\mu\text{m}$, and $30\mu\text{m}$ are shown in Figure 6 for all sources (upper set of three curves), and for sources located beyond redshift $z = 8$ (lower set of three curves). Although the $15\mu\text{m}$ counts are somewhat below those at $6\mu\text{m}$, the $30\mu\text{m}$ and $6\mu\text{m}$ counts are comparable. This follows directly from the dip in the spectra near $15\mu\text{m}$ (see Fig. 2). For the highest-redshift sources, the advantage of going to longer wavelengths is increased, with nearly an order of magnitude more sources at the 100nJy threshold at $30\mu\text{m}$ than at $6\mu\text{m}$. A considerable number of $z > 8$ galaxies, $\sim 30\text{arcmin}^{-2}$, are detectable at $30\mu\text{m}$ at 100nJy .

3.2. Confusion Noise

The potentially large number of detectable sources raises the important question of confusion. For an instrument whose angular resolution elements have an effective solid angle $\Delta\Omega$, one can define the confusion limit such that a source at this flux corresponds to (say) a 3σ fluctuation of the unresolved background due to all fainter sources. The critical surface density of background sources according to this definition depends on the slope of the counts (see, e.g., equation 8.26 in Franceschini 2000). The slope

we find in the flux range $\sim 10 - 10^4$ nJy is close to $d \log N / d \log F \approx -1$ (see Figs 4 and 6), implying that confusion limits sets in at the surface density of 1 source per ~ 9 beams.

For the MIR version of *TPF*, the effective beam-size is 0.25 arcsec^2 , and hence this instrument would be confusion limited at the source surface density of $\sim 0.4 \text{ arcsec}^{-2}$. This limit is shown as the dotted line in Figure 4. Although *TPF* is an interferometer with high resolution and exquisite nulling, the beam-size reflects the total collecting area of the side-lobes, and is relatively large⁴

For reference, we note that the effective size for the resolution element on *SIRTF* at $\sim 8 \mu\text{m}$ is $\sim 1.4 \text{ arcsec}^2$ (Simpson & Eisenhardt 1999), and our models would predict a confusion limit of $\sim 1 \mu\text{Jy}$ (in rough agreement, though somewhat higher, than the estimate by Simpson & Eisenhardt 1999 of $0.5 \mu\text{Jy}$, based on the extrapolated model number counts of Franceschini et al. 1991). For *NGST*, the size of the resolution element in the wavelength range $\sim 1 - 3.5 \mu\text{m}$ is much smaller, 0.0025 arcsec^2 (see Gillett & Mountain 1998), and the predicted counts at shorter wavelengths are also somewhat lower than at Mid-IR; based on Figure 3, we do not expect source confusion to be a problem down to 1nJy.

As can be seen from Figures 4 and 6, this surface density is reached near $\sim 100 \text{ nJy}$, i.e. close to the requisite target flux to detect Earth-like planets at 10 pc. High redshift galaxies can cause other problems for *TPF*. The surface density of galaxies at the confusion limit implies that in 1 out of 10 pointings, a galaxy with $F_\nu \sim 100 \text{ nJy}$ may be detected within the *TPF* beam. Every detected planet can therefore have upto 10% chance of being a mis-identified galaxy. Whether this is a significant contamination will, of course, depend on the rate at which planets are discovered by *TPF*. The unresolved background could also require greater uv-plane coverage to obtain an unambiguous image. We emphasize that none of these problems are likely to be show-stoppers for *TPF*: even for the maximum allowed surface density, repeat observations can be used to eliminate confusion-related problems.

4. CONCLUSIONS

Deep mid-infrared observations of the universe could reveal a new population of ultra-faint, high-redshift ($z > 3$) dusty starburst galaxies that are the progenitors of present-day spheroids or bulges. Although at a flux level of $\sim 100 \text{ nJy}$ these sources are beyond the reach of current instruments, the new population could be uncovered by *SIRTF* and *NGST*, and it could also constitute background noise for *TPF*. We used a simplified semi-analytic galaxy formation scheme to quantify the mid-infrared galaxy counts in an extreme model, designed to maximize the number of detectable sources down to a few nJy, while being consistent with various existing constraints. The model incorporates the formation of heavily dust-enshrouded stellar populations at high redshift.

Our results show that a new population could turn up at a flux level of $\sim 100 \text{ nJy}$. The sources would have typical halo masses of $\sim 10^{11} M_\odot$ (corresponding to $\sim 2\sigma$ peaks of the density field), redshifts $z > 3$ (with a significant tail at $z \gtrsim 8$), and ages $\sim 3 \times 10^8 \text{ yr}$. The models predict upto 0.4 galaxies/arcsec² at the threshold of 100 nJy at $6 \mu\text{m}$, with a comparable or larger surface densities at longer MIR wavelengths, especially at the highest redshifts. These results indicate that high-redshift galaxies could potentially necessitate repeat observations with *TPF*. However, the discovery of these faint sources would be a unique and direct probe of the earliest galaxies, and a combination of several wavelengths should provide insight into their formation mechanism.

We thank Gian Luigi Granato and Laura Silva for help with the use of their program GRASIL, and Rodger Thompson for helpful commentary on the NICMOS data. We also thank Peng Oh and Gian Luigi Granato for useful comments, and the Princeton TPF group for stimulating discussions. ZH was supported by NASA through the Hubble Fellowship grant HF-01119.01-99A, awarded by the Space Telescope Science Institute, which is operated by the Association of Universities for Research in Astronomy, Inc., for NASA under contract NAS 5-26555. ELT was supported by the NSF grant AST98-02802 and DNS was supported by the NASA grant NAG5-7154.

REFERENCES

- Barkana, R., & Loeb, A. 2001, Physics Reports, in press, astro-ph/0010468
 Binney, J., & Tremaine, S. 1987, Galactic Dynamics, Princeton Univ. Press, Princeton, NJ
 Bruzual, G., & Charlot, S. 2000, unpublished. The models are available from the anonymous ftp site ftp.ias.edu.
 Charlot, S., & Fall, S. M. 2000, ApJ, 539, 718
 Clements, D. L., Desert, F.-X., Franceschini, A., Reach, W. T., Baker, A. C., Davies, J. K., & Cesarsky, C. J. 1999, A&A, 346, 383
 Devriendt, J. E. G., & Guiderdoni, B. 2000, A&A, 363, 851
 Devriendt, J. E. G., Guiderdoni, B., & Sadat, R. 1999, A&A, 350, 381
 Dey, A., Spinrad, H., Stern, D., Graham, J. R., Chaffee, F. 1998, ApJ, 498, L93
 Draine, B. T., & Lee, H. M. 1984, ApJ, 285, 89
 Dwek, E. 2001, in "The Extragalactic Infrared Background and its Cosmological Implications", proc. of IAU Symp. 204, eds. M. Harwit and M. G. Hauser, in press, preprint astro-ph/01005363
 Eisenstein, D. J., & Hu, W. 1999, ApJ, 511, 5
 Fan, X., et al. 1999, AJ, 118, 1
 Fan, X., et al. 2000, AJ, 119, 1
 Fan, X., et al. 2001, in preparation
 Franceschini, A., Toffolatti, L., Mazzei, P., Danese, L., & De Zotti, G. 1991, A&ASS, 89, 285
 Franceschini, A. 2000, in "Galaxies at High Redshift", proc. of the XI. Canary Island Winter School of Astrophysics, eds. F. Sanchez, I. Perez-Fournon, M. Balcells, F. Moreno-Insertis, Cambridge University Press
 Franceschini, A., Aussel, H., Bressan, A., Cesarsky, C. J., Danese, L., De Zotti, G., Elbaz, D., Granato, G. L., Mazzei, P., & Silva, L. 1997, preprint astro-ph/9707080
 Gillett, F. C., & Mountain, M. 1998, in Science with the NGST, ASP Conference Series Vol. 133, ed. E. P. Smith & A. Koratkar, p. 42
 Gordon, K. D., Calzetti, D., & Witt, A. N. 1997, ApJ, 487, 625
 Guiderdoni, B., Hivon, E., Bouchet, F. R., & Maffei, B. 1998, MNRAS, 295, 877
 Haiman, Z., Abel, T., & Rees, M. J. 2000, ApJ, 534, 11
 Haiman, Z., & Loeb, A. 1997, ApJ, 483, 21
 Haiman, Z., & Loeb, A. 1998, ApJ, 503, 505
 Haiman, Z., & Spaans, M. 1999, ApJ, 518, 138
 Haiman, Z., Spaans, M., & Quataert, E. 2000, ApJL, 537, 5
 Haiman, Z., Thoul, A., & Loeb, A. 1996, ApJ, 464, 523 (HTL96)
 Hu, E. M., McMahon, R. G., & Cowie, L. L. 1999, ApJ, 522, L9
 Jenkins, A., Frenk, C. S., White, S. D. M., Colberg, J. M., Cole, S.,

⁴See the TPF Handbook at http://tpf.jpl.nasa.gov/library/tpf_book/index.html.

- Evrard, A. E., Couchman, H. M. P., Yoshida, N. 2001, MNRAS, 321, 372
- Kauffmann, G., & White, S. D. M. 1993, MNRAS, 261, 921
- Lacey, C. G., & Cole, S. 1993, MNRAS, 262, 627
- Leitherer, C., et al. 1999, ApJS, 123, 3
- Navarro, J. F., Frenk, C. S., & White, S. D. M. 1997, ApJ, 490, 493
- Navarro, J. F., & Steinmetz, M. 1997, ApJ, 478, 13
- Oh, S. P., & Haiman, Z., & Rees, M. J. 2001, ApJ, 553, 73
- Press, W. H., & Schechter, P. L. 1974, ApJ, 181, 425
- Puget, J. L., Léger, A., & Boulanger, F. 1985, A&A, 142, L19
- Wechsler, R. H., Somerville, R. S., Bullock, J. S., Kolatt, T. S., Primack, J. R., Blumenthal, G. R., Dekel, A. 2001, ApJ, 554, 85
- Serabyn, G. et al. 1999, "A Mid-Infrared Camera for the Next Generation Space Telescope", a report to NASA available at http://ngst.gsfc.nasa.gov/public_docs.html
- Sheth, R., Mo, H. J., & Tormen, G. 2001, ApJ, 323, 1
- Silva, L., Granato, G. L., Bressan, A., & Danese, L. 1998, ApJ, 509, 103
- Silva, L., Granato, G. L., Lacey, C., & Baugh, C. M. 1999, in "Evolution of Galaxies on Cosmic Timescales", proceedings of conference held at Puerto de la Cruz, Spain, December 1998, preprint astro-ph/9903350
- Simpson, C., & Eisenhardt, P. 1999, PASP, 111, 691
- Spinrad, H., Stern, D., Bunker, A. J., Dey, A., Lanzetta, K., Yahil, A., Pascarelle, S., & Fernández-Soto, A. 1998, AJ, 117, 2617
- Stern, D., Spinrad, H., Eisenhardt, P., Bunker, A. J., Dawson, S., Stanford, S., & Elston, R. 2000, ApJ, 533, L75
- Stanev, T., & Franceschini, A. 1998, ApJ, 494, L159
- Thompson, R. I., Storrie-Lombardi, L. J., Weymann, R. J., Rieke, M. J., Schneider, G., Stobie, E., & Lytle, D. 1999, ApJ, 117, 17
- Tumlinson, J., & Shull, J. M. 2000, ApJ, 528, L65
- Weymann, R. J., Stern, D., Bunker, A., Spinrad, H., Chaffee, F. H., Thompson, R. I., & Storrie-Lombardi, L. J. 1998, ApJ, 505, L95
- Whitmore, B. C., Kirshner, R. P., & Schechter, P. L. 1979, ApJ, 234, 68
- Williams, R. E., et al. 1996, AJ, 112, 1335
- Zheng, W., et al. 2000, AJ, 120, 1607